Acoustic receptivity of a boundary layer to Tollmien–Schlichting waves resulting from a finiteheight hump at finite Reynolds numbers

A. H. Nayfeh and O. N. Ashour

Articles you may be interested in

Stabilization of Tollmien–Schlichting waves by finite amplitude optimal streaks in the Blasius boundary layer
Phys. Fluids 14, L57 (2002); 10.1063/1.1493791

Optimal control of Tollmien–Schlichting waves in a developing boundary layer
Phys. Fluids 13, 2087 (2001); 10.1063/1.1378035

Boundarylayer receptivity due to a wall suction and control of Tollmien–Schlichting waves
Phys. Fluids A 4, 1206 (1992); 10.1063/1.858239

Effect of streamwise vortices on Tollmien–Schlichting waves in growing boundary layers
Phys. Fluids 30, 1005 (1987); 10.1063/1.866298

Sound and Tollmien–Schlichting waves in a Blasius boundary layer
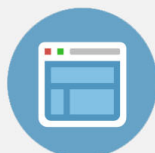Phys. Fluids 21, 2112 (1978); 10.1063/1.862119

Acoustic receptivity of a boundary layer to Tollmien–Schlichting waves resulting from a finite-height hump at finite Reynolds numbers

A. H. Nayfeh and O. N. Ashour
*Department of Engineering Science and Mechanics, Virginia Polytechnic Institute and State University,
Blacksburg, Virginia 24061-0219*

The acoustic receptivity of a boundary layer to Tollmien–Schlichting (T–S) waves resulting from a finite-height hump at finite Reynolds numbers is investigated. The steady flow is calculated using an interacting boundary-layer (IBL) scheme that accounts for viscous/inviscid interactions. The unsteady flow is written as the sum of a Stokes wave and a traveling wave generated due to the interaction of the Stokes flow with the steady disturbance resulting from the hump. The traveling wave is governed by a set of nonhomogeneous equations, which is a generalization of the Orr–Sommerfeld equation. The solution of these nonhomogeneous equations is projected onto the quasiparallel eigenmode using the quasiparallel adjoint. This leads to a nonhomogeneous equation with variable coefficients governing the amplitude and phase of the T–S wave. Results are presented for the amplitude variation and the receptivity at finite Reynolds numbers. The results are in good agreement with the experimental results of Saric, Hoos, and Radeztsky [*Boundary Layer Stability and Transition to Turbulence* (ASME, New York, 1991), FED No. 114, pp. 17–22] for all tested hump heights at the two-tested sound pressure levels. Application of this paper's theory to small humps yields results that agree with those of Choudhari and Streett [Phys. Fluids A **4**, 2495 (1992)], and Crouch [Phys. Fluids A **4**, 1408 (1992)]. Application of suction is shown to reduce the receptivity resulting from the hump.

I. INTRODUCTION

The term receptivity was first introduced by Morkovin[1] in the late 1960s to describe the response of a laminar flow-field to disturbances and the mechanisms by which disturbances are internalized in the boundary layer. Basically, the laminar–turbulent transition of the boundary layer can be separated into three stages: the generation of linear instability waves, the linear growth of these waves, and finally the nonlinear breakdown of the laminar flow and the origin of turbulence. The receptivity problem (being connected to the first stage) has recently become the focus of study of many researchers. This can be easily understood when we examine the numerous applications of this phenomenon in aerospace and mechanical engineering.

In principle, transition can be delayed by controlling any of the three stages. However, due to the violent nature of the nonlinear breakdown stage, it is most advantageous to influence transition by suppressing the generation and/or linear amplification processes. In the past, laminar flow technology has focused on means to reduce the linear growth of disturbances. This was due to the lack of knowledge concerning the generation processes. The various techniques used can be grouped as natural laminar flow (NLF), in which the airfoil shape is chosen to maintain favorable pressure gradients, laminar flow control (LFC), in which wall suction, heating, or cooling is utilized to enhance the stability of the boundary layer, and hybrid, in which a combination of NLF and LFC is used.

Although these techniques have shown success in extending the laminar flow region, there is a hidden danger in utilizing some of them. It should be noted that, when a transition delay technique is introduced, the influence of this technique on the first stage must also be considered. For example, suction strips may enhance the receptivity to free-stream acoustic waves, thereby negating some of the benefits obtained. Thus an understanding of the receptivity (i.e., how and where the instabilities are generated) is essential for attacking these instabilities at the root and possibly eliminating them.

In order for an external disturbance to generate an instability wave, energy must be transferred to the unsteady motion in the boundary layer at an appropriate combination of frequency and wavelength. In general, free-stream disturbances have well-defined propagation speeds, and hence the spatial spectrum at a given temporal frequency is concentrated at specific wave numbers, which are substantially different from the wave numbers of the instability waves.

Earlier studies of the effect of external disturbances on transition have been primarily experimental. Notable contributions include the experiments of Leehey and Shapiro,[2] Kachanov et al.,[3] Aizin and Polyakov,[4] and Dovgal et al.[5] Recently, Saric et al.[6] experimentally investigated the influence of a roughness element on the acoustic receptivity of a boundary layer. They took the precautions necessary for the sensitive measurements related to receptivity experiments. They found that the receptivity coefficient increases linearly with hump height until the height exceeds the lower-deck height where it shows a large deviation from linear behavior. Also, Dovgal and Kozlov[7] experimentally studied the effect of different hump shapes and sizes on the boundary-layer receptivity to acoustic disturbances. Their results show a significant enhancement of the natural instability waves due to the presence of acoustic disturbances.

The major question is the mechanism responsible for making the boundary layer receptive to its disturbance envi-

ronment. In other words, how the unsteady free-stream disturbance wavelength is transformed to the wavelength of the boundary-layer instability wave. In low-speed flows, the wavelength of the free-stream disturbances (acoustics, vortical) is much larger than that of the instability wave in the boundary layer. Therefore, the free-stream disturbance wavelength must be modified to match that of the instability wave by a certain mechanism. The pioneering work of Goldstein and Ruban has contributed to an understanding of the nature of this mechanism.

Goldstein[8,9] and Ruban[10] showed by using the high-Reynolds number asymptotic theory (linearized triple deck) that receptivity occurs in regions where the mean flow of the boundary layer exhibits rapid changes in the streamwise direction. This means that the classical quasiparallel steady boundary layer does not have the short length scale required for this modulation process. Furthermore, they showed that such regions can be grouped into two categories: leading-edge regions and regions where the boundary layer is forced to adjust rapidly. Examples of the latter include surface irregularities, such as humps and steps, and changes in the wall boundary-layer conditions, such as suction, blowing, and heating.

This analysis is valid only in a region around the lower branch because the triple-deck structure is valid there. However, for wall nonhomogeneity locations close to the upper branch, it will not be easy to apply the same theory because one would, then, have to ascertain the relative influence of the forcing within all of the five asymptotic subregions present in the upper-branch structure.[11]

Using the triple-deck theory of Goldstein,[8,9] Heinrich et al.[12] examined the receptivity for a range of free-stream disturbances, which include convected gusts. They considered the effects of gust orientation angle on an isolated semi-infinite plate and found that the receptivity is maximum for gusts whose wave direction is perpendicular to the plate surface. Kerschen and Choudhari[13] analyzed some receptivity problems encountered in laminar-flow control (LFC), including suction through a porous surface. They showed that short-scale variations in the admittance of the porous surface can also scatter energy directly from the acoustic wave to the instability wave.

Bodonyi et al.[14] extended the triple-deck framework of Goldstein and Ruban to study the effect of larger hump heights, where mean-flow perturbations generated by the wall hump are no longer small compared to the unperturbed mean flow. They used finite differences to solve the nonlinear triple-deck equations governing the mean flow. The unsteady problem is, however, still solved using the linearized triple-deck equations for infinite Reynolds numbers. Bodonyi and Duck[15] solved the linearized unsteady triple-deck problem due to the interaction between a small free-stream disturbance and a small localized suction strip on a flat plate. Again, the mean-flow (steady) problem was solved by using the nonlinear triple-deck structure to account for large values of the wall-suction parameter.

The triple-deck framework, which is based on a single-term asymptotic expansion in the limit of infinite Reynolds number in the neighborhood of branch I, reduces the Rey-

nolds number and frequency to a single parameter, thus disabling the study of frequency effects at different Reynolds numbers. Choudhari and Streett[16] and Crouch[17] generalized the asymptotic theory of Goldstein and Ruban to account for finite values of the Reynolds number. They utilized the classical Orr–Sommerfeld theory to predict the receptivity to small-amplitude surface nonuniformities. They expanded the flow in the region of receptivity as a regular perturbation series in terms of the small parameters corresponding to the amplitudes of the surface nonhomogeneity and the free-stream acoustic wave. The zeroth-order mean flow is the unperturbed, quasiparallel boundary layer. The solution of this problem is found by solving the steady Orr–Sommerfeld equation with nonhomogeneous boundary conditions. The next higher-order terms consist of short-scale perturbations due to the presence of the surface irregularity, which satisfy nonhomogeneous forms of the linear partial differential equations corresponding to disturbance propagation in a parallel shear flow. Since the parallel-flow equations are independent of the streamwise coordinate, these partial differential equations can be reduced to ordinary ones by taking a Fourier transform in the streamwise direction, and the instability wave amplitude can then be determined as the residue corresponding to the appropriate pole of the Fourier transform solution. These analyses are valid for finite Reynolds numbers, near or away from branch I. They also allow the study of frequency effects at different Reynolds numbers.

The accuracy of the approach of Choudhari and Streett[16] and Crouch[17] is limited by the assumptions of small hump heights and locally parallel mean flow. In fact, their results agree with the experimental results of Saric et al.[6] only for small hump heights. In this paper, we propose an alternate approach for analyzing the disturbance field generated by an acoustic forcing over a flat plate with a finite-height surface hump at a finite Reynolds number. The basic (mean) flow is calculated by using interacting boundary layers (IBL), thus accounting for viscous/inviscid interactions and separation bubbles. The unsteady motion is assumed to be the sum of a Stokes wave and a traveling wave. The traveling wave is governed by a set of nonhomogeneous partial differential equations with variable coefficients. The nonhomogeneity reflects the interaction of the Stokes wave with the steady disturbance caused by the roughness element. The solution of this set of equations is projected onto the quasiparallel eigenmode by using the quasiparallel adjoint. The result is a first-order complex-valued nonhomogeneous ordinary-differential equation governing the amplitude and phase of the traveling wave. Solutions of this equation provide variation of the amplitude of the traveling wave with streamwise distance, which is used to determine the receptivity coefficients. The results are in good agreement with the experimental results of Saric et al.[6] for all tested hump heights at the two tested sound pressure levels.

II. MEAN FLOW

The two-dimensional laminar boundary-layer flow over the plate and the roughness element is determined by solving the interacting boundary-layer equations.[18,19] These equations account for the upstream influence through the interac-

A. H. Nayfeh and O. N. Ashour

tion of the viscous flow with the inviscid flow outside the boundary layer. Moreover, they are also capable of capturing separation bubbles without difficulties.[20] Recently, Hsiao and Pauley[21] compared the results obtained by solving for the flow with a small separation bubble using three different methods: triple-deck theory, interactive boundary layers (IBL), and the full Navier–Stokes equations. Among these three methods, IBL was found to be the most suitable method for solving a flow with a small separation bubble since it accurately determines the boundary-layer separation solution at low Reynolds numbers and requires less programing efforts and CPU time than the Navier–Stokes computations. Solutions are obtained by using a second-order finite-difference method in which the grid spacings acknowledge the scaling predicted by the triple-deck theory in the interaction region.

We consider a two-dimensional incompressible steady flow over a smooth two-dimensional hump on a flat plate. The shape of the hump in terms of dimensionless variables is given by

$$Y_1 = \frac{y^*}{L^*} = \left(\frac{h^*}{L^*}\right) f(\eta) = Hf(\eta), \tag{1}$$

where

$$\eta = (x^* - x_m^*)/b^* = (X - X_m)/b. \tag{2}$$

and $X = x^*/L^*$ with L^* being the distance from the leading edge of the plate to the center of the hump. We present numerical results for a cubic hump defined by

$$f(\eta) = \begin{cases} 1 - 3\eta^2 + 2|\eta|^3 & \text{if } |\eta| \leq 1, \\ 0 & \text{if } |\eta| > 1 \end{cases} \tag{3}$$

and a quartic hump defined by

$$f(\eta) = \begin{cases} (1 - \eta^2)^2 & \text{if } |\eta| \leq 1, \\ 0 & \text{if } |\eta| > 1. \end{cases} \tag{4}$$

The mean flow is governed by the boundary-layer equations

$$U \frac{\partial U}{\partial X} + V_1 \frac{\partial U}{\partial Y_1} = U_e \frac{dU_e}{dX} + \frac{1}{\text{Re}} \frac{\partial^2 U}{\partial Y_1^2}, \tag{5}$$

$$\frac{\partial U}{\partial X} + \frac{\partial V_1}{\partial Y_1} = 0, \tag{6}$$

where U_e is the streamwise edge velocity and Re is the Reynolds number given by Re $= U_\infty^* L^*/\nu^*$. The no-slip and no-penetration conditions demand that

$$U = V_1 = 0 \quad \text{at } Y_1 = Hf(\eta). \tag{7}$$

If there is suction or blowing at the wall, then the boundary condition on V_1 is replaced by $V_1 = V_w$ at the wall, where V_w is the physical velocity at the wall normalized with respect to U_∞^*. Away from the wall,

$$U \to U_e \quad \text{as } Y_1 \to \infty. \tag{8}$$

To solve for the mean flow, we use the Prandtl transposition theorem and let

$$Y = Y_1 - Hf[\eta(X)] \quad \text{and} \quad V = V_1 - HU \frac{df}{dX} [\eta(X)]. \tag{9}$$

The governing equations and boundary conditions then become

$$U \frac{\partial U}{\partial X} + V \frac{\partial U}{\partial Y} = U_e \frac{dU_e}{dX} + \frac{1}{\text{Re}} \frac{\partial^2 U}{\partial Y^2}, \tag{10}$$

$$\frac{\partial U}{\partial X} + \frac{\partial V}{\partial Y} = 0, \tag{11}$$

$$U = V = 0 \quad \text{at } Y = 0, \tag{12}$$

$$U \to U_e \quad \text{as } Y \to \infty. \tag{13}$$

Next, we introduce the Levy–Lees variables, specialized for incompressible flow,

$$\xi = \int_0^X U_e \, dX, \quad \eta = Y U_e \sqrt{\frac{\text{Re}}{2\xi}}, \tag{14}$$

$$\bar{F} = \frac{U}{U_e}, \quad \bar{V} = \frac{2\xi}{U_e} \left(\bar{F} \frac{\partial \eta}{\partial X} + V \sqrt{\frac{\text{Re}}{2\xi}}\right) \tag{15}$$

and rewrite the problem as

$$2\xi \bar{F} \bar{F}_\xi + \bar{V} \bar{F}_\eta + \beta(\bar{F}^2 - 1) - \bar{F}_{\eta\eta} = 0, \tag{16}$$

$$2\xi \bar{F}_\xi + \bar{V}_\eta + \bar{F} = 0, \tag{17}$$

$$\bar{F} = \bar{V} = 0 \quad \text{at } \eta = 0, \tag{18}$$

$$\bar{F} \to 1 \quad \text{as } \eta \to \infty, \tag{19}$$

$$\bar{F} = \bar{F}(\xi_0, \eta) \quad \text{at } \xi = \xi_0, \tag{20}$$

where ξ_0 corresponds to a location upstream of the interaction region and

$$\beta = \frac{2\xi}{U_e} \frac{dU_e}{d\xi}. \tag{21}$$

With U_e specified by the inviscid flow over the hump surface, Eqs. (16)–(20) represent a conventional boundary-layer theory. However, due to the large change in the boundary conditions, which causes strong viscous/inviscid coupling and an upstream influence, these equations fail to provide a solution, and one needs to use a triple-deck formulation, interacting boundary layers (IBL), or a Navier–Stokes solver. For smooth imperfections, IBL can be used accurately to determine the flow field. In this work, we use an IBL formulation. The interaction law relates the edge velocity U_e to the scaled displacement surface $\delta_1 \sqrt{\text{Re}}$ as

$$\delta = \delta_1 \sqrt{\text{Re}} = \frac{\sqrt{2\xi}}{U_e} \int_0^\infty (1 - \bar{F}) d\eta, \tag{22}$$

$$U_e = \bar{U}_e + \frac{1}{\pi} \int_{\text{LE}}^\infty \frac{1}{X - t} \frac{d}{dt} [\bar{U}_e \delta(\text{Re})^{-1/2}] dt, \tag{23}$$

where $\bar{U}_e$ is the inviscid surface velocity in the absence of the boundary layer, which is given by

A. H. Nayfeh and O. N. Ashour   3707

$$\bar{U}_e = 1 + \frac{1}{\pi} \int_{\text{LE}}^{\infty} \frac{1}{X-t} \, d \, \frac{(Hf)}{dt} \, dt. \qquad (24)$$

Equations (16)–(20) are solved simultaneously with the interaction law (23). We follow Nayfeh et al.[18] and assume δ to vary linearly over a differencing interval, thereby yielding a second-order accurate scheme. For more details on this formulation, we refer the reader to Nayfeh et al.[18]

III. STABILITY ANALYSIS

We consider the two-dimensional spatial stability of the basic flow determined by the IBL code. We follow classical stability theory and introduce dimensionless quantities using the fixed length scale $\delta_r = \sqrt{(\nu^* L^*/U_\infty^*)}$, the outer velocity U_∞^*, and the free-stream density ρ^*. In classical stability theory, the results are normally presented using the length scale $\delta_x = \sqrt{\nu^* x^*/U_\infty^*}$, which is proportional to the local boundary-layer thickness on a flat plate. This results in a moving Reynolds number

$$R = U_\infty^* \delta_x/\nu^* = \sqrt{U_\infty^* x^*/\nu^*}. \qquad (25)$$

To study the two-dimensional stability of a certain mean flow, we superimpose on it an unsteady disturbance to obtain the total flow

$$\hat{u}(x,y_1,t) = U(x,y_1) + \bar{u}(x,y_1,t), \qquad (26)$$

$$\hat{v}(x,y_1,t) = V_1(x,y_1) + \bar{v}_1(x,y_1,t), \qquad (27)$$

$$\hat{p}(x,y_1,t) = P(x,y_1) + \bar{p}(x,y_1,t), \qquad (28)$$

where U, V_1, and P are the basic streamwise and transverse velocities and pressure, respectively, and $y_1 = y^*/\delta_r$. Substituting Eqs. (26)–(28) into the Navier–Stokes equations, subtracting the mean-flow quantities, linearizing the resulting equations, and using the Prandtl-transposition theorem as in Eq. (9), we obtain

$$\frac{\partial \bar{u}}{\partial x} + \frac{\partial \bar{v}}{\partial y} = 0, \qquad (29)$$

$$\frac{\partial \bar{u}}{\partial t} + U \frac{\partial \bar{u}}{\partial x} + \bar{v} \frac{\partial U}{\partial y} + \frac{\partial \bar{p}}{\partial x} - \frac{1}{\sqrt{\text{Re}}} \nabla^2 \bar{u} + \bar{u} \frac{\partial U}{\partial x} + V \frac{\partial \bar{u}}{\partial y}$$
$$= hf' \frac{\partial \bar{p}}{\partial y}, \qquad (30)$$

$$\frac{\partial \bar{v}}{\partial t} + U \frac{\partial \bar{v}}{\partial x} + \bar{v} \frac{\partial V}{\partial y} + \frac{\partial \bar{p}}{\partial y} - \frac{1}{\sqrt{\text{Re}}} \nabla^2 \bar{v} + \bar{u} \frac{\partial V}{\partial x} + V \frac{\partial \bar{v}}{\partial y}$$
$$= -hf' \left(\frac{\partial \bar{u}}{\partial t} + U \frac{\partial \bar{v}}{\partial x} + V \frac{\partial \bar{u}}{\partial y} + \bar{v} \frac{\partial U}{\partial y} + \bar{u} \frac{\partial U}{\partial x} \right)$$
$$- 2hf'' \bar{u} U, \qquad (31)$$

$$\bar{u} = \bar{v} = 0 \quad \text{at} \quad y = 0, \qquad (32)$$

$$\bar{v} \to 0 \quad \text{as } y \to \infty, \qquad (33)$$

$$\bar{u} \to \epsilon e^{-i\omega t} + \text{c.c.} \quad \text{as } y \to \infty, \qquad (34)$$

where ω and ϵ are the nondimensional frequency and amplitude of the acoustic disturbance and c.c. stands for the complex conjugate.

To solve Eqs. (29)–(34), we introduce a transformation to convert the problem from that of solving a homogeneous set of equations with nonhomogeneous boundary conditions into that of solving a nonhomogeneous set of equations subject to homogeneous boundary conditions. To this end, we let

$$[\bar{u}, \bar{v}, \bar{p}] = [u_a, v_a, p_a] + [u, v, p], \qquad (35)$$

where u_a, v_a, and p_a are unsteady acoustic free-stream disturbances and u, v, and p are generated Tollmein–Schlicting (T–S) waves. The acoustic disturbances are taken in the form of the Stokes flow

$$u_a = \epsilon[(1 - e^{-\theta y}) e^{-i\omega t}] + \text{c.c.}, \qquad (36)$$

$$v_a = 0, \qquad (37)$$

$$p_a = \epsilon i \omega x e^{-i\omega t} + \text{c.c.}, \qquad (38)$$

where $\theta = \sqrt{-i\omega \sqrt{\text{Re}}}$. Substituting Eqs. (35)–(38) into Eqs. (29)–(34) yields

$$\frac{\partial u}{\partial x} + \frac{\partial v}{\partial y} = 0, \qquad (39)$$

$$\frac{\partial u}{\partial t} + U \frac{\partial u}{\partial x} + v \frac{\partial U}{\partial y} + \frac{\partial p}{\partial x} - \frac{1}{\sqrt{\text{Re}}} \nabla^2 u$$
$$= -\left(u \frac{\partial U}{\partial x} + V \frac{\partial u}{\partial y} \right) + hf' \frac{\partial p}{\partial y} - \frac{\partial U}{\partial x} u_a - V \frac{\partial u_a}{\partial y}, \qquad (40)$$

$$\frac{\partial v}{\partial t} + U \frac{\partial v}{\partial x} + v \frac{\partial V}{\partial y} + \frac{\partial p}{\partial y} - \frac{1}{\sqrt{\text{Re}}} \nabla^2 v$$
$$= -\left(u \frac{\partial V}{\partial x} + V \frac{\partial v}{\partial y} \right) - hf' \left(\frac{\partial u}{\partial t} + \frac{\partial u_a}{\partial t} + U \frac{\partial u}{\partial x} + V \frac{\partial u}{\partial y} \right.$$
$$\left. + V \frac{\partial u_a}{\partial y} + v \frac{\partial U}{\partial y} + \frac{\partial U}{\partial x} \right) - 2hf'' U(u + u_a) - u_a \frac{\partial V}{\partial x}. \qquad (41)$$

The boundary conditions become

$$u = v = 0 \quad \text{at } y = 0, \qquad (42)$$

$$u, v \to 0 \quad \text{as } y \to \infty. \qquad (43)$$

The solution of Eqs. (39)–(43) in the vicinity of the hump is very complex. Fortunately, to determine the receptivity, we do not need to solve these equations. Instead, we project the disturbance onto the local T–S wave and let

$$[u, Du, v, p]^T(x,y,t) = B(x) \zeta(x,y) e^{i \int \alpha \, dx - i\omega t} + \text{c.c.}$$
$$+ \chi(x,y,t), \qquad (44)$$

where the ζ_n are components of the solution of the quasiparallel problem

$$D\zeta = \Lambda \zeta, \qquad (45)$$

$$\zeta_1 = \zeta_3 = 0 \quad \text{at } y = 0, \qquad (46)$$

$$\zeta_n \to 0 \quad \text{as } y \to \infty, \qquad (47)$$

A. H. Nayfeh and O. N. Ashour

where $D = d/dy$,

$$\Lambda = \begin{bmatrix} 0 & 1 & 0 & 0 \\ \Gamma & 0 & \sqrt{Re}\,DU & i\alpha\sqrt{Re} \\ -i\alpha & 0 & 0 & 0 \\ 0 & -i\alpha/\sqrt{Re} & -\Gamma/\sqrt{Re} & 0 \end{bmatrix} \quad (48)$$

and

$$\Gamma = \alpha^2 + i\sqrt{Re}(\alpha U - \omega). \quad (49)$$

Hence,

$$B(x) = e^{-i\int \alpha\,dx + i\omega t} \int_0^\infty [u, Du, v, p]\zeta^* \, dy, \quad (50)$$

where ζ^* is the adjoint vector of the T–S wave and

$$\int_0^\infty \chi^T \zeta^* \, dy = 0. \quad (51)$$

Substituting Eq. (44) into Eqs. (39)–(43), we obtain residuals e_1, e_2, and e_3. Assuming that these residuals are orthogonal to the adjoint ζ_1^*, ζ_2^*, ζ_3^*, and ζ_4^* of the T–S wave, we obtain an equation for B in the form

$$\frac{dB}{dx} = \bar{h}(x)B + \epsilon k(x)e^{-i\int \alpha\,dx}, \quad (52)$$

where $\bar{h}(x)$ and $k(x)$ are defined in the Appendix.

We let

$$B = Ae^{-i\int \alpha\,dx}, \quad (53)$$

where A is the total complex wave amplitude, in Eq. (52) and obtain

$$\frac{dA}{dx} = (i\alpha + \bar{h})A + \epsilon k. \quad (54)$$

In Eq. (54), $\bar{h}(x)$ is due to nonparallelism and $\epsilon k(x)$ is due to the acoustic disturbance. In the case of parallel flow, $\bar{h} \equiv 0$ and α and k are constants. For quasiparallel flow, $\bar{h} = 0$ but α and k vary with streamwise position. This is the case treated in this paper.

Equations (45)–(47) and their adjoint are solved numerically using the IMSL library subroutine DBVPFD, which utilizes finite-difference methods. The results are then used to calculate $\bar{h}(x)$ and $k(x)$. Equation (54) is then integrated using a Runge–Kutta scheme with appropriate initial conditions.

IV. RESULTS AND DISCUSSION

The results are presented using the varying Reynolds number $R = \sqrt{Re_x} = \sqrt{U_\infty^* x^*/\nu^*}$, as the streamwise variable. The nondimensional disturbance frequency ω is related to the dimensional frequency by $F = \omega/R = 2\pi f^* \nu^*/U_\infty^{*2}$, where f^* is the dimensional frequency in hertz.

The analysis provides the total amplitude of the traveling wave resulting from the receptivity process. The total amplitude is the physical quantity that can be measured in an experiment. It depends on both the linear growth rate and the receptivity, resulting from the roughness element.
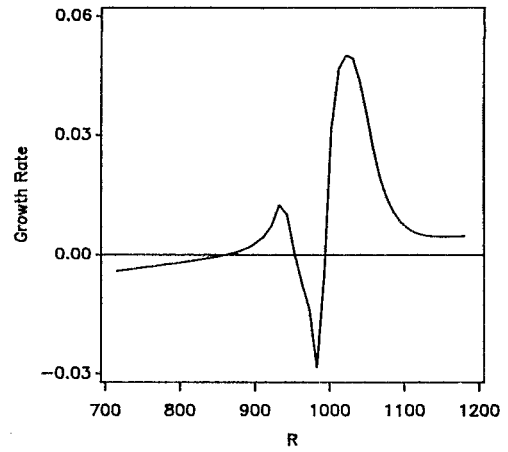

FIG. 1. Streamwise distribution of the growth rate $(-\alpha_i)$ for a hump centered at $x = 1$ ($R = 983$): $h/b = 0.031$, $b = 0.1$, and $F = 25 \times 10^{-6}$.

In Fig. 1, we show the quasiparallel growth rate $-\alpha_i$ for a cubic hump having the height $h = h^*/L^* = 0.0031$ and centered at $x_m = 1$, where L^* is the location corresponding to $Re = 9.66 \times 10^5$ at the center of the hump. The symmetric hump extends from $x_l = 0.9$ to $x_r = 1.1$. The frequency F in this case is equal to 25×10^{-6}, which is the most dangerous frequency for the Blasius flow.[18] It is clear that the presence of the hump increases the growth rate until $x = x_l$, decreases it in the interval (x_l, x_m), and increases it again in the interval (x_m, x_r).

In Fig. 2, we show the forcing term $k(x)$ in Eq. (54) for $\epsilon = 0.01$. It is clear that this term attains its maximum at a location just downstream of the hump, where the mean-flow gradient attains its maximum. At locations far upstream or far downstream of the hump, the forcing term $k(x)$ is negligibly small. The case of a flat plate (without the hump) is also shown in Fig. 2 for comparison. Clearly, the hump has a significant influence. It has both an upstream as well as a downstream influence. These influences are captured in the present quasiparallel formulation. At locations far upstream or far downstream of the hump, the two curves coincide.
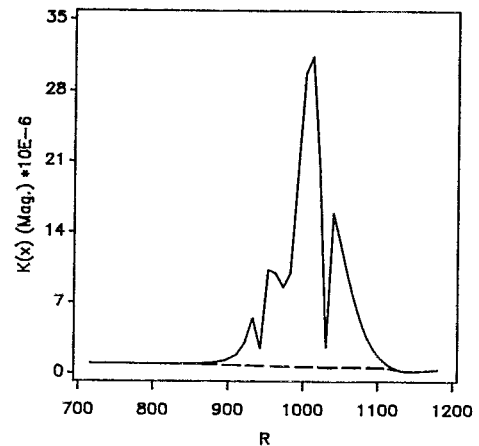

FIG. 2. The forcing term in Eq. (54) for the hump of Fig. 1, $F = 25 \times 10^{-6}$, and $\epsilon = 0.01$: (—) cubic hump and (---) flat plate.

A. H. Nayfeh and O. N. Ashour   3709
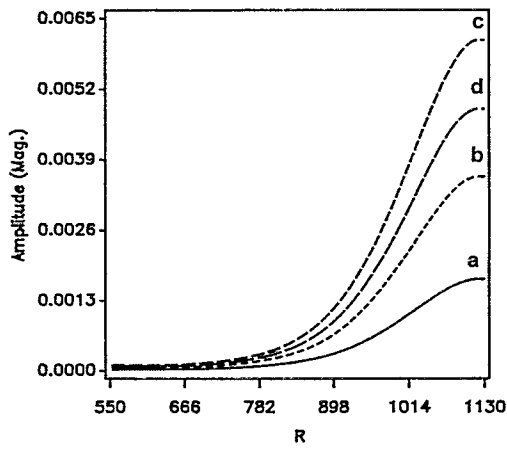
FIG. 3. Influence of the initial conditions on the amplitude of the disturbance for one of the humps tested by Saric et al.[6] for $F=49.34\times10^{-6}$ and 90 dB. The hump is rectangular with height 100 μm and width 25 mm. The initial conditions are (a) $A_0=3\times10^{-5}$ and $\phi_0=0$, (b) $A_0=6\times10^{-5}$ and $\phi_0=0$, (c) $A_0=6\times10^{-5}$ and $\phi_0=0.75$, and (d) $A_0=6\times10^{-5}$ and $\phi_0=1.2$.

A. Comparison with earlier studies and experiments

In this section, we compare the results obtained by our analysis with those obtained by Crouch[17] and Choudhari and Streett[16] and with the experiments of Saric et al.[6]

Saric et al.[6] provided detailed experimental results on the acoustic receptivity due to a 2-D rectangular hump, but after taking the precautions necessary for the sensitive receptivity measurements. The flat plate and leading edge had mirror-like finishes and the flow was insured to have a zero pressure gradient. The hump was placed across the span of the flat plate at $R=582$ and at a distance of 460 mm from the leading edge. The hump was built by using ultrathin uniform tapes of width 25 mm. Extreme care was taken when applying the tape across the entire 1.4 m span of the flat plate. They kept the hump width fixed and varied its height by adding more tapes. Measurements were conducted for two different sound pressure levels, namely, 90 and 100 dB. The eigenmodes and free-stream acoustic amplitudes were measured at a fixed downstream location in the neighborhood of branch II. To calculate the mean flow over the rectangular humps tested by Saric et al., we approximate the humps by two steps having a large slope of 20: a forward-facing step and a backward-facing step.

The experimentally obtained receptivity amplitude does not tend to zero as the hump height tends to zero, suggesting the presence of some a priori disturbance that is out of phase with the disturbance generated by the hump and the dependence of the receptivity amplitude on the initial conditions. To validate this observation, we perform calculations for several initial amplitudes and phases of the a priori present disturbance. In Fig. 3, we study the effect of changing the initial conditions A_0 and ϕ_0 on the evolution of the total amplitude for one of the cases investigated by Saric et al.[6] The roughness height is 100 μm and its width is 25 mm and the frequency $F=49.34\times10^{-6}$. The acoustic amplitude ϵ is 0.016%, which corresponds to a sound pressure level of 90 dB. The different cases studied are $A_0=3\times10^{-5}$ and $\phi_0=0$;
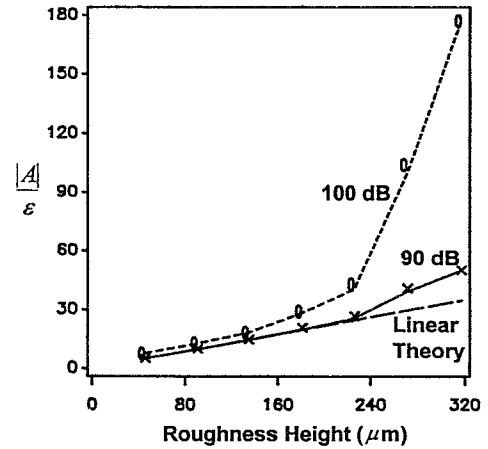

FIG. 4. Comparison between our results (solid and broken) and the experimental results of Saric et al. for the 90 dB sound pressure level ($\times$) and the 100 dB sound pressure level (0) and the linear theory of Choudhari and Streett[16] and Crouch (———).[17]

$A_0=6\times10^{-5}$ and $\phi_0=0$; $A_0=6\times10^{-5}$ and $\phi_0=0.75$; and $A_0=6\times10^{-5}$ and $\phi_0=1.2$. The effect of changing the initial amplitude or the phase on the amplitude of the wave generated by the hump is clearly shown. As the initially created wave comes into the receptivity region, it will enhance or reduce the wave created by receptivity depending on the relative phases.

To quantitatively compare our theory with the experimental results of Saric et al., we need to specify the initial conditions. Inspection of the experimental results clearly shows that the initial conditions when the sound pressure level is 90 dB are different from the initial conditions when the sound pressure level is 100 dB. Therefore, in the absence of measured initial conditions, for each sound pressure level, we choose initial conditions to match the receptivity amplitude for one hump height and use these initial conditions to compute the receptivity amplitude at all other hump heights. The initial conditions that have been chosen are $A_0=3\times10^{-5}$ and $\phi_0=0$ for the 90 dB case and $A_0=4.1\times10^{-5}$ and $\phi_0=0.75$ for the 100 dB case.

In Fig. 4, we show a comparison between our theory and the experiment for the receptivity amplitude A/ϵ as a function of the dimensional height h^* at the frequency $F=49.34\times10^{-6}$ for the two tested sound pressure levels. The agreement between our theoretical results and the experimental results is excellent for both sound pressure levels. The figure also compares the linear theoretical results of Crouch[17] and Choudhari and Streett[16] with the experimental results and our results. It is clear that the agreement between the linear theory and the experiment is very good for hump heights less than 225 μm for the 90 dB case. The experimental results show that the receptivity at 90 dB is a nonlinear function of the roughness height for h^* greater than 225 μm. On the other hand, for the 100 dB case, the receptivity is a nonlinear function of the roughness height for h^* greater than 150 μm. In fact, Saric et al.[6] pointed out that nonlinear effects become more dominant when the reattachment length of the separation bubble significantly exceeds the hump
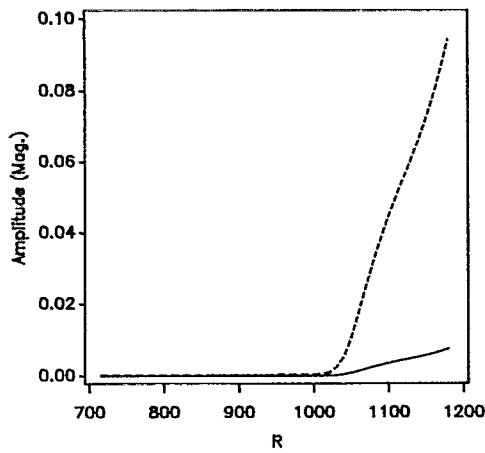
A. H. Nayfeh and O. N. Ashour

FIG. 5. Streamwise evolution of the total amplitude for the hump of Fig. 1 and $F=25\times10^{-6}$: (—) $\epsilon=0$ and (---) $\epsilon=0.01$.

height. In this case, our theoretical results indicate that the reattachment lengths at $h^*=270$ and $317~\mu$m are greater than the hump height by a factor of 6 and 8, respectively. Because of the parallel assumption, the theory of Choudhari and Streett[16] and Crouch[17] predicts the same curve at both of the 90 and 100 dB sound pressure levels. The parallel theory cannot account for the initial conditions. On the other hand, our quasiparallel theory can account for the influence of the initial conditions and hence two curves are predicted by using two sets of initial conditions.

B. Effect of hump height and shape

It is clear from the preceding section that the initial conditions strongly influence the evolution of the amplitude of the generated wave. Large growth rates may result from some initial conditions, or equivalently, from the birth of the instability waves. Therefore, to evaluate the effects of the hump characteristics, acoustic frequency, and laminar flow control mechanisms on the receptivity, we need to specify the initial conditions. In what follows, we choose the arbitrary initial conditions $A_0=1\times10^{-4}$ and $\phi_0=0$ and evaluate these effects.

To investigate the influence of the hump height on the receptivity to free-stream disturbances, we selected a cubic hump defined by Eq. (3), fixed its width at $2b=0.2$, and located its center at an L^* corresponding to $R=983$. In their work, Nayfeh et al.[18] concluded that one of the geometrical factors of the imperfection that govern the instability is the height-to-width ratio (h^*/b^*). This finding was also reached by Cebeci and Ergan[22] and Eli and Van Dam.[23] In this paper, we consider the cases $h^*/b^*=0.01$, 0.015, 0.019, 0.021, 0.026, 0.031, 0.037, and 0.05. Masad and Nayfeh[24] studied the stability of separating boundary layers. They showed that, for the considered cubic hump, the height at which the flow starts to separate (incipient separation) is 0.0021. This corresponds to a ratio of $h^*/b^*=0.021$. The frequency in these calculations was fixed at $F=25\times10^{-6}$. The total amplitude for each of the above cases was calculated in the presence of acoustic forcing. The case shown in Fig. 5 cor-
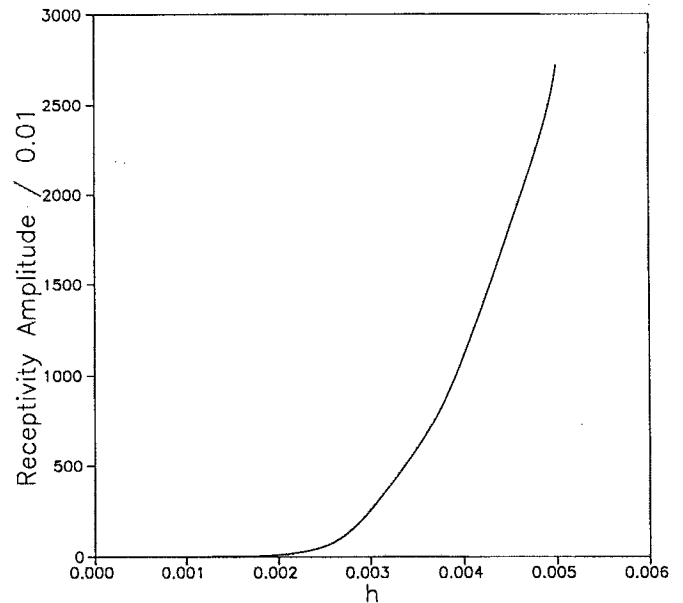

FIG. 6. Variation of the receptivity amplitude A/ϵ with the hump height h: $x_m=1(R=983)$, $F=25\times10^{-6}$, $b=0.1$, and $\epsilon=0.01$.

responds to $h^*/b^*=0.031$, where we have plotted the amplitudes in the presence and absence of acoustic forcing, for comparison. It is obvious that the presence of the acoustic forcing enhances the growth of the wave by dramatically increasing the rate of this growth.

In Fig. 6, we show the receptivity amplitude A/ϵ, calculated at the branch II location, for all the above cases. Clearly, the receptivity amplitudes for humps that do not induce separation (i.e., $h^*/b^*<0.021$) are very small compared to those for humps that induce separation. Again, this emphasizes the importance of studying boundary-layer separation. Saric et al.[6] pointed out that the receptivity mechanism becomes nonlinear when an extended separation occurs; that is, when the reattachment length significantly exceeds the height of the hump. This separation may form a free-shear layer that can exhibit its own instability, thereby altering the receptivity observed in the linear region. We note that, for very large hump sizes that could induce massive separation, IBL formulations breakdown and a Navier–Stokes solver has to be used.

Next, we investigate the influence of the hump shape. To this end, we considered a quartic hump, defined by Eq. (4). The heights of both humps were fixed at 0.0031. The results obtained in the two cases are shown in Fig. 7. The quartic hump appears to provide a more receptive environment. However, the two curves are very close to each other.

C. Effect of hump location

In Fig. 8, we show the influence of changing the location of a hump having a height-to-width ratio of 0.031 on the amplitude evolution with streamwise location for $F=25\times10^{-6}$. The hump was placed at the five different locations $x_m=0.75$, 0.86, 1, 2.19, and 2.86, corresponding to $R=851$, 911, 983, 1454, and 1662, respectively. For loca-
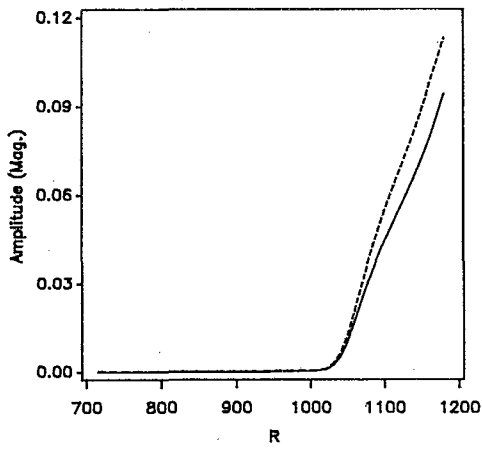
FIG. 7. Streamwise evolution of the total amplitude for cubic and quartic humps located at $R=983$, $h/b=0.031$, $F=25\times10^{-6}$, and $\epsilon=0.01$: (—) cubic hump and (---) quartic hump.

FIG. 9. Effect of hump location on the receptivity amplitude A/ϵ: $h/b=0.031$, $b=0.1$, $\epsilon=0.01$, and $F=25\times10^{-6}$.

tions around branch I of the neutral stability curve of the Blasius flow ($R=910.4$), the boundary layer is more receptive to its disturbance environment. For comparison, the different locations considered are also indicated on the Blasius neutral stability curve in the figure. For all locations near or upstream of branch I, the amplitude grows rapidly in a short distance, namely, the interaction region of the hump. For locations downstream of branch I, the hump appears to be smaller compared to the thickness of the boundary layer, and hence its effect appears to be smaller.

In Fig. 9, we plot the receptivity amplitude A/ϵ for different locations of the hump. The two neutral stability points of the Blasius flow corresponding to branches I and II, respectively, are also indicated on the x axis. Clearly, the receptivity at the location indicated by point 3 on the neutral stability curve in Fig. 8, which is just downstream of branch I, is the most significant.
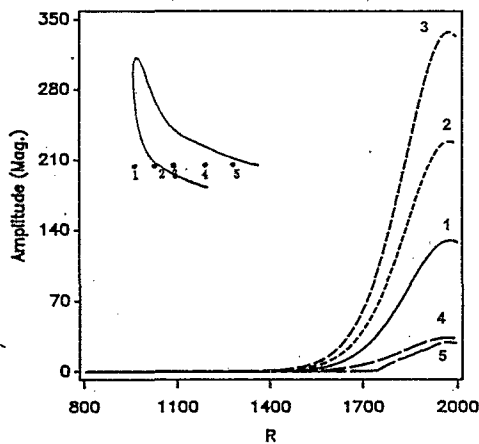
D. Effect of acoustic frequency

After studying the factors characterizing the hump, we turn our attention to the factors characterizing the free-stream acoustic disturbances, namely, their frequencies. We considered the following frequencies: $F=20$, 25, 30, 35, 40, 45, and 50×10^{-6}. We calculated the total amplitude of the generated wave for each of the above cases in the presence of the acoustic disturbance. The results are shown in Fig. 10. Clearly, the receptivity amplitude A/ϵ increases with increasing frequency.

FIG. 8. Effect of hump location on the streamwise variation of the total amplitude when $h/b=0.031$, $F=25\times10^{-6}$, and $\epsilon=0.01$: 1–5 correspond to $x_m=0.75$, 0.86, 1.0, 2.19, and 2.86.
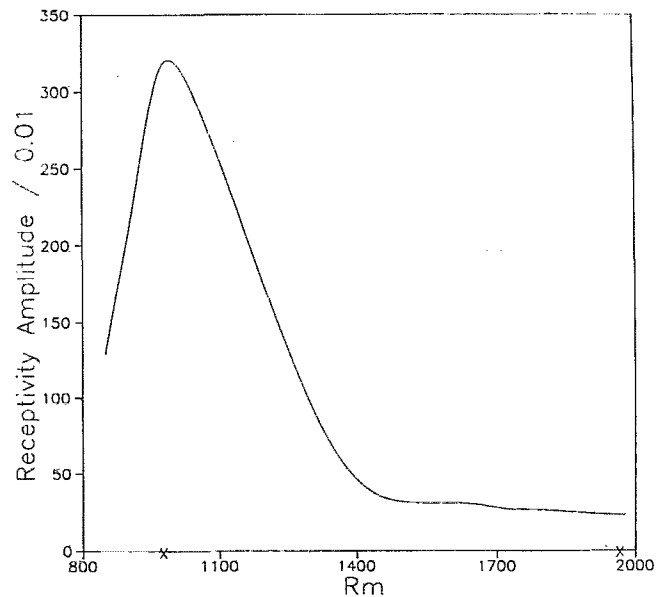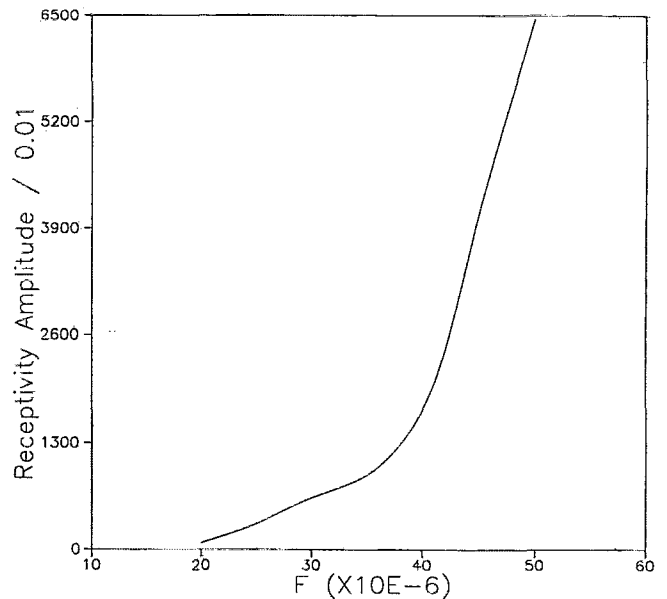

FIG. 10. Effect of the acoustic frequency on the receptivity amplitude A/ϵ for the cubic hump of Fig. 1 with $h/b=0.031$.
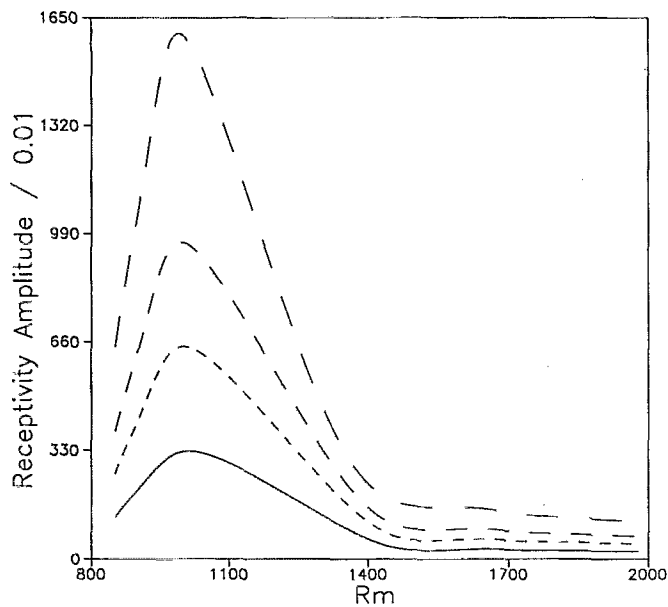
FIG. 11. Effect of hump location on the receptivity amplitude A/ϵ at different frequencies: $h/b=0.031$, $b=0.1$, and $\epsilon=0.01$: $F=$(——) 25×10^{-6}, (---) 30×10^{-6}, (——) 35×10^{-6}, and (———) 45×10^{-6}.

Next, we investigate the effect of the hump location for different frequencies. To this end, we plot the receptivity amplitude A/ϵ at different locations of the hump for $F=25$, 30, 35, and 45×10^{-6}. The results are shown in Fig. 11. It is clear that, as the frequency increases, the hump location that yields the maximum receptivity amplitude A/ϵ moves downstream of branch I.

In Fig. 12, we plot variation of the receptivity amplitude A/ϵ with hump height for different frequencies. The four
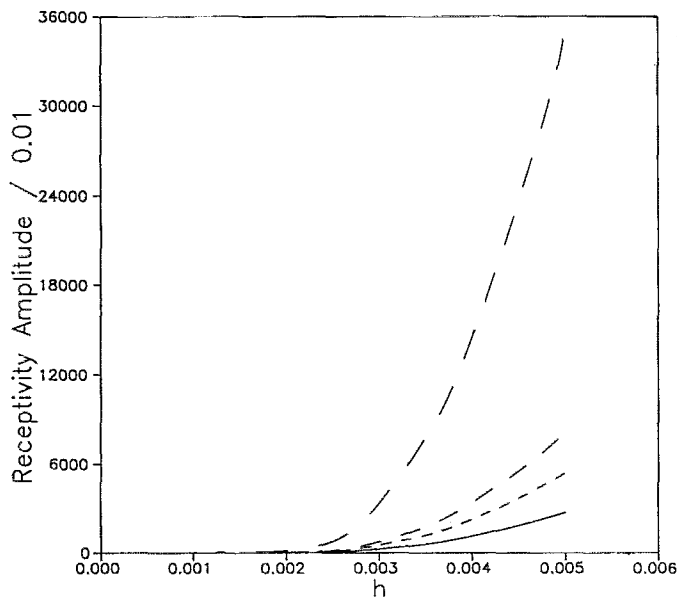

FIG. 12. Effect of hump height on the receptivity amplitude A/ϵ at different frequencies: $b=0.1$ and $\epsilon=0.01$: $F=$ (——) 25×10^{-6}, (---) 30×10^{-6}, (——) 35×10^{-6}, and (———) 45×10^{-6}.
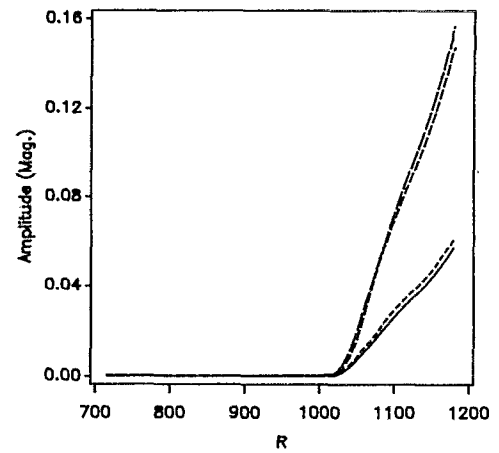

FIG. 13. Effect of nonparallelism on the evolution of the total amplitude for the same hump of Fig. 1: (–) $\epsilon=0$ parallel, (---) $\epsilon=0$ nonparallel, (———) $\epsilon=0.01$ parallel, and (— —) $\epsilon=0.01$ nonparallel.

cases considered are $F=25$, 30, 35, and 45×10^{-6}. All graphs exhibit the same general behavior. The receptivity amplitude grows at a larger rate for heights exceeding the one that causes incipient separation ($h=0.0021$). However, as the frequency increases, the slope of the graph after $h=0.0021$ increases, indicating that separation effects on the receptivity coefficient are larger at higher frequencies.

E. Effect of nonparallelism

Now, we study the effect of nonparallelism on the receptivity problem. The results are shown in Fig. 13 for the case $F=25\times10^{-6}$, where we have plotted the amplitudes corresponding to the cases of natural instability based on the parallel assumption, the case of natural instability based on the nonparallel assumption, the case with acoustic forcing based on the parallel assumption, and the case with acoustic forcing based on the nonparallel assumption. Although the nonparallelism results in a larger amplitude for both cases of natural and forced instabilities, the increase is small and negligible. So, it does not justify the amount of work needed to calculate the nonparallel terms. This agrees with previous results performed for the cases of a flat plate[25] and a backward-facing step,[26] where the complete Navier–Stokes equations were numerically integrated using a finite-difference scheme. The growth rates obtained are in excellent agreement with those obtained by a quasiparallel stability analysis. Hence, the nonparallel effects are insignificant and the quasiparallel-flow assumption can be used without loss of accuracy.

F. Effect of wall blowing/suction

As pointed out in the Introduction, the receptivity occurs in regions where the boundary layer is forced to adjust rapidly. After studying the receptivity due to a hump, we now turn to study the effects of other mechanisms, such as blowing and suction. In Fig. 14, we plot the total amplitude of the instability wave resulting from receptivity due to wall blowing at the frequency $F=25\times10^{-6}$. In this case, the blowing
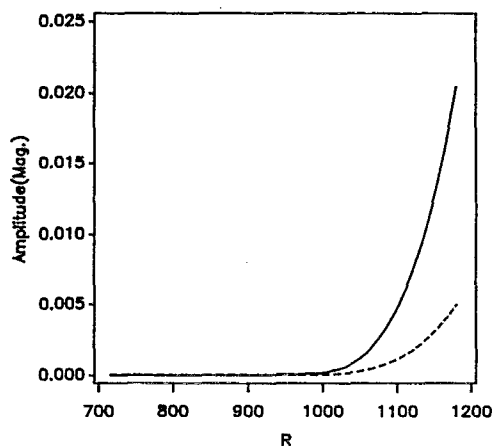
FIG. 14. Effect of wall blowing on the evolution of the total amplitude for flow conditions, as in Fig. 2. The blowing strip is centered at $x=1$ ($R=983$), $F=25\times10^{-6}$, $b=0.1$, and $V_w=6.0\times10^{-4}$: (---) $\epsilon=0$ and (—) $\epsilon=0.01$.

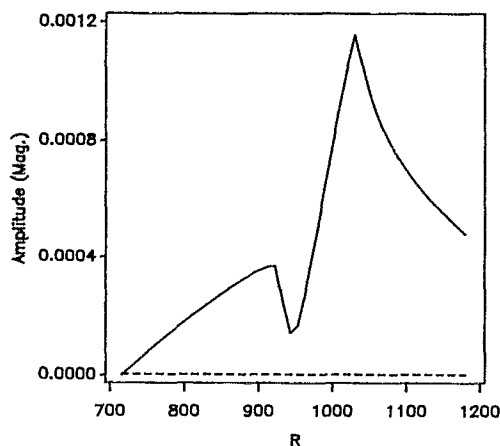
FIG. 15. Effect of wall suction on the evolution of the total amplitude. The suction strip is centered at $x=1$($R=983$), $F=25\times10^{-6}$, $b=0.1$, and $V_w=-6.0\times10^{-4}$: (---) $\epsilon=0$ and (—) $\epsilon=0.01$.

strip has a width of 0.2 and is centered at $x=1$ ($R=983$). The magnitude of the physical blowing velocity V_w normalized with respect to U_∞^* is 6.0×10^{-4}. The evolution of the natural instability wave is also shown for comparison. Again, we note that wall blowing enhances the receptivity process. The location at which the amplitude starts to be significant is also shifted upstream.

To study the effect of wall suction, we changed the sign of V_w. In this case, the results are dramatically different from those obtained in the case of blowing. Here, the amplitude is given an initial jump that starts to decay farther downstream in an oscillatory way. This can be attributed to the fact that suction is stabilizing, and hence it tends to stabilize or damp the generated wave. To eliminate these oscillations, we set the initial conditions equal to zero to increase the effect of the forcing term on the process. The results are shown in Fig. 15, where we plot the generated amplitude for the cases of natural and forced instabilities. By comparing these results to those obtained for the blowing case, we conclude that the receptivity due to blowing is more significant than that due to suction.

G. Effect of suction on the receptivity of humps

Next, we study the influence of applying suction on the receptivity of humps. In Fig. 16, we show the results for a hump of height $h=0.0031$ at the frequency $F=25\times10^{-6}$ in the absence and presence of a suction strip with $V_w=-6.0\times10^{-4}$. The location of the suction strip coincides with the hump location ($0.9\leq x\leq1.1$). The results show clearly that application of wall suction reduces the destabilizing influence and receptivity of the hump.

Next, we investigate the optimum location of the suction strip; that is, the location that minimizes the effect of the hump on the receptivity of acoustic disturbances and the growth of the generated waves. We considered the five locations: $L_1(0.9\leq x\leq1.1)$, $L_2(0.8\leq x\leq1.0)$, $L_3(1.0\leq x\leq1.2)$, $L_4(0.85\leq x\leq1.05)$, and $L_5(0.95\leq x\leq1.15)$. The results are shown in Fig. 17. Location L_5, where the center

of the suction strip is at $x=1.05$, is the optimum location for minimizing the receptivity. On the other hand, location L_2, where the center of the suction strip is at $x=0.9$, is the least efficient location for placing the suction strip. This is expected because the gradients of the mean-flow quantities are positive in the interval (x_m,x_r). Hence, placing the suction strip in this interval will minimize these gradients and hence minimize the receptivity process.

V. CONCLUDING REMARKS

An analysis of the receptivity to acoustic disturbances due to the presence of a finite-height surface hump at finite Reynolds on a flat plate is conducted. The mean flow is calculated using interacting boundary layers. The unsteady disturbance is expressed as the sum of a Stokes wave and a traveling wave generated due to the interaction of the Stokes wave and the steady flow generated by the hump. The solution of the resulting nonhomogeneous equations is projected
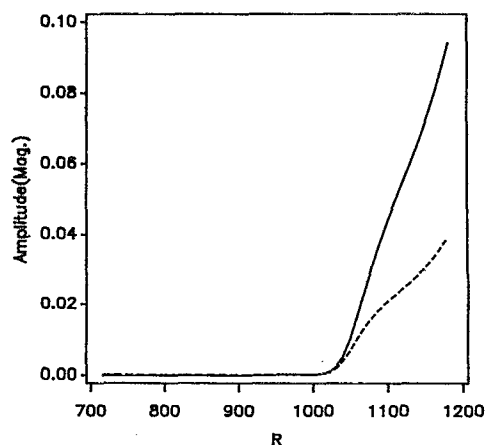

FIG. 16. Effect of a hump with suction on the evolution of the total amplitude for the same hump conditions, as in Fig. 1. The suction strip is centered at $x=1$($R=983$): $F=25\times10^{-6}$, $b=0.1$, and $\epsilon=0.01$: (—) $V_w=0$ and (---) $V_w=-6.0\times10^{-4}$.
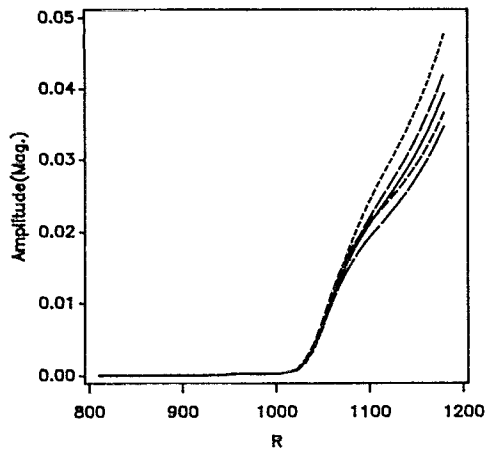
A. H. Nayfeh and O. N. Ashour

FIG. 17. Effect of suction strip location on the evolution of the total amplitude for the flow conditions in Fig. 2, $h/b=0.031$, $b=0.1$, $F=25\times10^{-6}$, and $\epsilon=0.01$ (——) L1, (- - -) L2, (—- —-) L3, (———) L4, and (———————) L5.

onto the eigenmode of the quasiparallel problem by using the quasiparallel adjoint, resulting in a complex-valued first-order ordinary-differential equation governing the amplitude and phase of the disturbance. The amplitude of the generated wave depends on the initial conditions, the height, width, and location of the hump, and the acoustic frequency. The results are in excellent agreement with the experimental results of Saric *et al.*[6] for all tested hump heights at the two tested sound pressure levels. The results are also in agreement with the linear theory of Choudhari and Streett and Crouch for small hump heights. Application of suction through porous strips reduces the receptivity due to humps.

ACKNOWLEDGMENT

APPENDIX: COEFFICIENTS FOR EQ. (54)

$$f_1(x) = \int_0^\infty [\zeta_2^* \sqrt{\mathrm{Re}}(U\zeta_1 + \zeta_4) - \zeta_3^* \zeta_1 - U\zeta_4^* \zeta_3]\,dy,$$

$$f_2(x) = -\int_0^\infty \zeta_2^* \left[\sqrt{\mathrm{Re}}\, U\, \frac{\partial \zeta_1}{\partial x} + \sqrt{\mathrm{Re}}\, \frac{\partial \zeta_4}{\partial x} + \sqrt{\mathrm{Re}}\, \frac{\partial U}{\partial x} \zeta_1 \right.$$
$$\left. + \sqrt{\mathrm{Re}}\, V\zeta_2 + ihf'\alpha\zeta_2 + \Gamma hf'\zeta_3 \right] dy,$$

$$f_3(x) = \int_0^\infty \zeta_3^* \frac{\partial \zeta_1}{\partial x}\,dy,$$

$$f_4(x) = \int_0^\infty \zeta_4^* \left[U\frac{\partial \zeta_3}{\partial x} + VD\zeta_3 + \zeta_3 DV - i\omega hf'\zeta_1 \right.$$
$$\left. + i\alpha U hf'\zeta_1 + hf'DU\zeta_3 + 2hf''U\zeta_1 \right] dy,$$

$$f_5(x) = -\int_0^\infty \zeta_2^* \sqrt{\mathrm{Re}} \left[\frac{\partial U}{\partial x}(1 - e^{-\theta y}) + \theta V e^{-\theta y} \right] dy,$$

$$\bar{h}(x) = [f_2(x) + f_3(x) + f_4(x)]/f_1(x),$$

$$k(x) = f_5(x)/f_1(x).$$

[1] M. V. Morkovin, "Critical evaluation of transition from laminar to turbulent shear layers with emphasis on hypersonically traveling bodies," AFFDL-TR-68-149, 1969.
[2] P. Leehey and P. J. Shapiro, "Leading-edge effect in laminar boundary-layer excitation by sound," *Proceedings of the IUTAM Symposium on Laminar–Turbulent Transition* (Springer-Verlag, Berlin, 1980), pp. 321–331.
[3] Y. S. Kachanov, V. V. Kozlov, and V. Y. Levchenko, "Occurrence of Tollmien–Schlichting waves in the boundary layer under the effect of external perturbations," Fluid Dyn. **13**, 704 (1979).
[4] L. B. Aizin and M. F. Polyakov, "Acoustic generation of Tollmien–Schlichting waves over local unevenness of surface immersed in stream," Preprint No. 17, Akad. Nauk SSSR, Siberian Division, Institute of Theoretical and Applied Mechanics, Novosibirsk, 1979.
[5] A. V. Dovgal, Y. S. Kachanov, V. V. Kozlov, V. Y. Levchenko, and V. P. Maksimov, "Origin of perturbations in boundary layers," Akad. Nauk SSSR, Sieberian Division, Institute of Theoretical and Applied Mechanics, 4-22, Novosibirsk, 1979 (in Russian) (translated in NASA TM-77986, 1986).
[6] W. Saric, J. Hoos, and R. Radeztsky, "Boundary-layer receptivity of sound with roughness," *Boundary Layer Stability and Transition to Turbulence*, edited by D. C. Reda, H. L. Reed, and R. Kobayashi (American Society of Mechanical Engineers, New York, 1991), FED No. 114, pp. 17–22.
[7] A. Dovgal and V. Kozlov, "Hydrodynamic instability and receptivity of small scale separation regions," in *Laminar–Turbulent Transition*, edited by D. Arnal and R. Michel (Springer-Verlag, Berlin, 1990), pp. 523–531.
[8] M. E. Goldstein, "The evolution of Tollmien–Schlichting waves near a leading edge," J. Fluid Mech. **127**, 59 (1983).
[9] M. E. Goldstein, "Scattering of acoustic waves into Tollmien–Schlichting waves by small streamwise variations in surface geometry," J. Fluid Mech. **154**, 509 (1985).
[10] A. I. Ruban, "On the generation of Tollmien–Schlichting waves by sound," Fluid Dyn. **19**, 709 (1985).
[11] R. J. Bodonyi and F. T. Smith, "The upper branch stability of the Blasius boundary layer," Proc. R. Soc. London Ser. A **375**, 65 (1981).
[12] R. A. Heinrich, M. Choudhari, and E. Kerschen, "A comparison of boundary-layer receptivity mechanisms," AIAA Paper No. 88-3758, 1988.
[13] E. Kerschen and M. Choudhari, "Boundary-layer receptivity at a suction surface-hard wall junction," Bull. Am. Phys. Soc. **30**, 1709 (1985).
[14] R. J. Bodonyi, W. J. Welch, P. W. Duck, and M. Tadjfar, "A numerical study of the interaction between free-stream disturbances and localized variations in surface geometry," J. Fluid Mech. **209**, 285 (1989).
[15] R. J. Bodonyi and P. W. Duck, "Boundary-layer receptivity due to a wall suction and control of Tollmien–Schlichting waves," Phys. Fluids A **4**, 1206 (1992).
[16] M. Choudhari and C. Streett, "A finite Reynolds-number approach for the prediction of boundary-layer receptivity in localized regions," Phys. Fluids A **4**, 2495 (1992).
[17] J. D. Crouch, "Localized receptivity of boundary layers," Phys. Fluids A **4**, 1408 (1992).
[18] A. H. Nayfeh, S. A. Ragab, and A. A. Al-Maaitah, "Effect of bulges on the stability of boundary layers," Phys. Fluids **31**, 796 (1988).
[19] R. T. Davis and M. J. Werle, "Progress on interacting boundary-layer computations at high Reynolds number," in *Numerical and Physical Aspects of Aerodynamic Flows*, edited by T. Cebeci (Springer-Verlag, Berlin, 1982), pp. 187–198.
[20] S. A. Ragab, A. H. Nayfeh, and R. C. Krishna, "Stability of compressible boundary layers over a smooth backward-facing step," AIAA Paper No. 90-1449, 1990.
[21] C. Hsiao and L. Pauley, "The accuracy of the triple-deck theory for marginal separation," *Separated Flows*, edited by J. C. Dutton and L. P. Purtell (American Society of Mechanical Engineers, New York, 1993), FED No. 149, pp. 199–208.

[22] T. Cebeci and D. Egan, "Prediction of transition due to isolated roughness," AIAA J. **27**, 870 (1989).

[23] S. Eli and C. P. Van Dam, "The influence of a laminar separation bubble on boundary-layer instability," AIAA Paper No. 91-3294, 1991.

[24] J. A. Masad and A. H. Nayfeh, "Stability of separating boundary layers," *The Fourth International Congress of Fluid Mechanics*, Alexandria, Egypt, 28–30 April 1992, pp. 260–278.

[25] H. Fasel and U. Konzlemann, "Non-parallel stability of a flat plate boundary layer using the complete Navier–Stokes equations," J. Fluid Mech. **221**, 311 (1990).

[26] H. Bestek, K. Gurber, and H. Fasel, "Direct numerical simulation of unsteady separated boundary-layer flows over smooth backward-facing steps," in *Notes on Numerical Fluid Mechanics*, edited by K. Gersten (1993), Vol. 40, pp. 73–80.

A. H. Nayfeh and O. N. Ashour